

Observation of ferrotoroidic domains in a metal

Takeshi Hayashida ^{1,2,*}, Ryusuke Misawa,² Manfred Fiebig ^{3,†} and Tsuyoshi Kimura ^{1,2,†}

¹*Department of Applied Physics, University of Tokyo, Bunkyo-ku, Tokyo 113-8656, Japan*

²*Department of Advanced Materials Science, University of Tokyo, Kashiwa, Chiba 277-8561, Japan*

³*Department of Materials, ETH Zurich, 8093 Zurich, Switzerland*



(Received 24 December 2023; accepted 12 February 2024; published 4 March 2024)

Ferrotoroidic order has recently been established as a new form of spontaneous long-range order. Its inherent magnetoelectric properties have the potential to be utilized for spintronics based on magnetization-free systems. While spintronics applications have been mostly discussed for conducting systems, the ferroic properties of ferrotoroidic order have been mainly studied in insulating materials thus far. Here we report on the observation of ferrotoroidic order in a rare-earth tetraboride, NdB_4 , that shows metallic conductivity and no spontaneous magnetization. Using optical second harmonic generation (SHG), we spatially resolve the formation, distribution, and behavior of the ferrotoroidic domains across the ordering temperature. Due to the interference between the domains with the opposite ferrotoroidic polarity, SHG signals cancel out at the domain boundaries, which enables us to image the ferrotoroidic domain pattern. This study opens the way to explore unique functionalities of ferrotoroidic domains in metals, such as an electric-current-induced domain switching.

DOI: [10.1103/PhysRevB.109.L100401](https://doi.org/10.1103/PhysRevB.109.L100401)

Ferrotoroidic order is characterized by a spontaneous vortex arrangement of magnetic dipoles, with the order parameter of the toroidal moment given by $\mathbf{T}^M \propto \sum_i \mathbf{r}_i \times \mathbf{m}_i$, where \mathbf{r}_i is the position vector of the magnetic dipole \mathbf{m}_i at the i site with reference to the high-symmetry point of the unit cell. Ferroic ordering of toroidal moments in crystals has been theoretically discussed since the 1980s [1–6]. An experimental observation of ferrotoroidic domains using optical second harmonic generation (SHG) [7] and a switching of the domains by applying electric and magnetic fields [8] in LiCoPO_4 have led to the recognition of ferrotoroidic order as the fourth primary ferroic state of matter [9]. Ferrotoroidic order simultaneously breaks space-inversion (P) and time-reversal (T) symmetries, resulting in the emergence of the linear magnetoelectric (ME) effect [6,10–13] and nonreciprocal optical phenomena [14–17], which have been studied extensively in insulating materials. By contrast, ferrotoroidic order has been much less investigated in metallic materials, even though the coupling between the electric current of a conductor and ferrotoroidic order has been theoretically discussed more than twenty years ago [4]. However, the recent surge of attention in magnetically compensated spintronics materials [18,19] has heightened the interest in ferrotoroidic order of metallic materials. For example, the relationship between the toroidal moment and current-induced antiferromagnetic domain switching has been investigated [20,21] in Mn_2Au [22] and CuMnAs [23] thin films. Furthermore, electric-current-induced magnetization has been discussed for ferrotoroidic metallic UNi_4B [24,25].

Since any functionality of a ferroic material roots in its domains, for potential applications of ferrotoroidic order in future spintronics devices, the observation of responses to external stimuli on the level of the domains is indispensable. Yet, before even considering the response of the domains to external stimuli, a method for the direct observation of ferrotoroidic domains in bulk metals needs to be accomplished. In this study, we therefore demonstrate the visualization of ferrotoroidic domains in metallic NdB_4 by optical SHG. We perform spatial distribution measurements of SHG signals in the setting sensitive to ferrotoroidic ordering, which is verified by the SHG anisotropy measurements.

NdB_4 is a rare-earth tetraboride crystallizing as a tetragonal system with the space group $P4/mbm$ [see Fig. 1(a) for the crystal structure] [26,27]. It exhibits the typical resistivity of a metal ($10^{-7} \Omega \text{ cm}$ at 2 K) [28]. Due to their geometrical frustration, some of the tetraborides exhibit noncollinear magnetic structures which break both P and T symmetries [29–31]. Recently, an optical ME effect in TbB_4 has been evidenced via the observation of nonreciprocal rotation of reflected light [32]. Thus, the rare-earth tetraborides constitute a good platform to explore properties due to P and T symmetry breaking in metallic systems. The Nd moments in NdB_4 order at $T_0 = 17.2 \text{ K}$, where a noncollinear magnetic structure shown in Figs. 1(b) and 1(c) develops [33–35]. Just below T_0 , the moments lie in the ab plane, and they start to tilt towards the c axis with decreasing temperature. The tilt angle at 3 K is about 17° [35]. However, no spontaneous magnetization is observed in the magnetically ordered phase [28]. The magnetic point group in this phase is $2'/m$ in which P , T , fourfold rotational, and mirror symmetries are broken. Due to the variety of symmetry breakings, NdB_4 exhibits three types of ferroic order: ferrotoroidic, ferroelastic, and ferroaxial [36–38]. Note that the ferrotoroidic order is leading in magnitude as it is

*thayashida@ap.t.u-tokyo.ac.jp

†These authors contributed equally to this work.

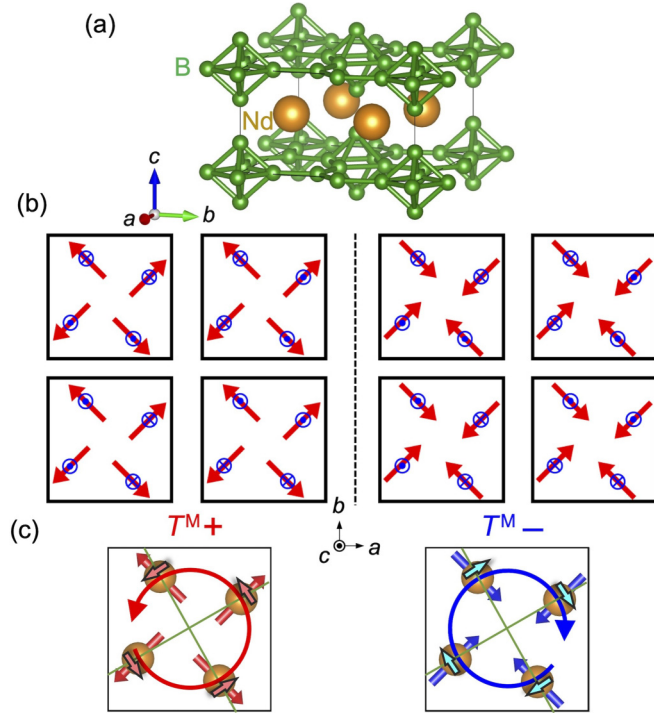


FIG. 1. (a) Crystal structure of NdB_4 . (b) The eight domain states allowed when including the out-of-plane magnetic moments. The red arrows denote in-plane magnetic moments which are related to ferrotoroidic order. The blue circles with a dot and cross in the center denote out-of-plane magnetic moments pointing up and down, respectively. The left (right) four panels show the domain states with T^{M+} (T^{M-}). (c) A pair of ferrotoroidic domain states (T^{M+} and T^{M-}) of NdB_4 . The red and blue arrows denote Nd magnetic moments. The red and blue circle arrows represent positive and negative toroidal moments, respectively. The green lines connect the center of the unit cell to the Nd atoms and are parallel to their position vector \mathbf{r}_i . The light red and blue arrows denote the projection of the magnetic moments into the plane normal to \mathbf{r}_i , contributing to the toroidal moment.

determined by the in-plane magnetic moments [red arrows in Fig. 1(b)], whereas the other orders are determined by the out-of-plane magnetic moments [blue arrows in Fig. 1(b)]. Hence, when the out-of-plane components are neglected, we have the point group $4/m'mm$ and ferrotoroidic order only. The toroidal moment points in the c axis direction, and the toroidal moment per unit cell volume is calculated as $0.012 \mu_B \text{ \AA}^{-2}$. Here we used the in-plane magnetic moment at a single Nd site $m_{\perp c} = 1.8 \mu_B$ at 7.0 K [35] and the lattice parameters $a = b = 7.2349 \text{ \AA}$ and $c = 4.1101 \text{ \AA}$ at 7.5 K [34]. The three different ferroic orderings result in a total of eight domain states as shown in Fig. 1(b). However, with the smallness of the out-of-plane components, one can focus on just a pair of ferrotoroidic domain states, T^{M+} and T^{M-} , which are related to one another by either P or T operations, as depicted in Fig. 1(c). The light red and blue arrows in Fig. 1(c) denote the projection of the magnetic moments on the in-plane normal to the position vector of each Nd moment, contributing to the toroidal moment. We note that NdB_4 undergoes two more magnetic transitions at 7.0 and 4.8 K, where the out-of-plane

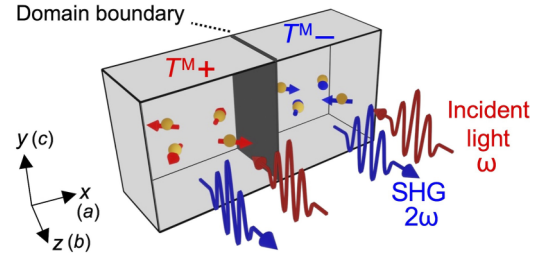


FIG. 2. The experimental setup for the SHG measurements on NdB_4 . Red- and blue-colored pulses denote incident fundamental and emitted SHG light, respectively. Although no difference in the SHG intensity between T^{M+} and T^{M-} is expected (see main text), destructive interference arises from SHG across different domains. Consequently, domain boundaries manifest as dark lines with diminished SHG intensity.

magnetic moments accompany an incommensurate modulation [35]. These transitions do not affect the in-plane magnetic moments constituting the ferrotoroidic order, however.

The breaking of P and T symmetries allows for SHG in the electric-dipole approximation [39], which is forbidden in the centrosymmetric phase temperature above T_0 and can thus provide background-free access to the ferrotoroidic state. The nonlinear polarization \mathbf{P} at frequency 2ω is induced by an incident electromagnetic light field \mathbf{E} at frequency ω and is described as

$$P_i(2\omega) = \varepsilon_0 \chi_{ijk} E_j(\omega) E_k(\omega), \quad (1)$$

where ε_0 is the vacuum permittivity and χ_{ijk} are the components of the SHG susceptibility tensor. In the magnetically ordered phase of NdB_4 with the point group $2'/m$, there is a total of ten independent tensor components: χ_{xxy} , χ_{yyy} , χ_{yxx} , χ_{zzy} , χ_{yyz} , χ_{xxx} , χ_{xyy} , χ_{yxy} , χ_{zxx} , and χ_{xzz} [40]. Here, we set the crystallographic a , c , and b axes in the tetragonal setting parallel to the orthogonal x , y , and z axes, respectively (see Fig. 2). Among the ten components, χ_{xxy} , χ_{yyy} , χ_{yxx} , χ_{zzy} , and χ_{yyz} derive from the in-plane ferrotoroidic ordering according to the point group $4/m'mm$, and their sign depends on the ferrotoroidic polarity, i.e., $\chi(T^{M+}) = -\chi(T^{M-})$. Thus, SHG from opposite domain states [left and right panels of Fig. 1(c)] exhibits a 180° phase difference, allowing for the detection of the domain structure [7,41]. The other five components are due to the out-of-plane magnetic moments. A SHG polarization analysis is capable of distinguishing between all of these components.

A single crystal of NdB_4 was grown by the floating-zone method using a furnace equipped with a laser diode that bears five laser heads arranged in a circumferential configuration (Quantum Design Japan L-FZ 2000) [42]. The obtained crystal was oriented using Laue x-ray diffraction and cut into plates with the widest faces perpendicular to the b axis. One of these plates was mechanically prepared using lapping films. For SHG measurements, an amplified Ti:sapphire laser with a pulse duration of 130 fs and a repetition rate of 1 kHz was used. An optical parametric amplifier converts the 800 nm emission to a wavelength of 1200 nm. The experiments were performed in a near-normal-incidence reflection geometry (angle of incidence $\leq 4^\circ$), and the SHG light emitted from the

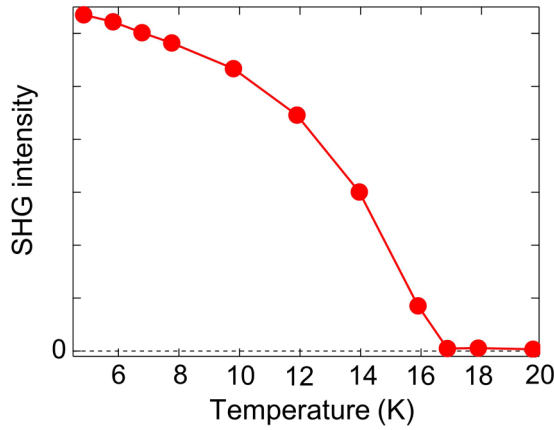


FIG. 3. Temperature dependence of the SHG intensity obtained in the setting where the polarization of the incident fundamental light (\mathbf{P}_ω) and that of the detected SHG light ($\mathbf{P}_{2\omega}$) were parallel to the y axis ($\mathbf{P}_\omega \parallel \mathbf{P}_{2\omega} \parallel y$).

tetragonal ac plane was detected with a photomultiplier tube detector or a liquid-nitrogen-cooled charge-coupled-device camera (see Fig. 2 for illustration). The laser fluence and the beam diameter were $10 \mu\text{J}$ and 1.5 mm , respectively. In this setting, the frequency-doubled polarization is expressed as

$$\mathbf{P}(2\omega) = \varepsilon_0 \begin{pmatrix} \chi_{xxx}E_x(\omega)^2 + 2\chi_{xxy}E_x(\omega)E_y(\omega) + \chi_{xyy}E_y(\omega)^2 \\ \chi_{yyy}E_y(\omega)^2 + 2\chi_{yyx}E_x(\omega)E_y(\omega) + \chi_{yxx}E_x(\omega)^2 \\ 0 \end{pmatrix}. \quad (2)$$

A commercial liquid-helium-operated cryostat (Janis SVT-400) was used to control sample temperature.

Figure 3 shows the temperature dependence of the SHG intensity, where the polarization of the incident fundamental light (\mathbf{P}_ω) and that of the detected SHG light ($\mathbf{P}_{2\omega}$) were both parallel to the y axis ($\mathbf{P}_\omega \parallel \mathbf{P}_{2\omega} \parallel y$). In this setting, one addresses the χ_{yyy} component, which, as mentioned, couples to the ferrotoroidic order. No SHG signal was observed above 17 K , suggesting that contributions from surface SHG are negligible. By contrast, a SHG signal was observed below 17 K , corresponding to the ferrotoroidic transition. Furthermore, the temperature dependence of the SHG signal was in good agreement with that of the intensity of the (110) reflection obtained by polarized neutron diffraction which corresponds to the in-plane magnetic order parameter [35], corroborating that SHG from the χ_{yyy} component successfully extracts the ferrotoroidic ordering in NdB_4 .

Next, we performed spatially resolved SHG measurements at 10 K ($< T_0$). Figure 4(a) shows the obtained SHG image in the polarization setting of $\mathbf{P}_\omega \parallel \mathbf{P}_{2\omega} \parallel y$. The SHG intensity is almost uniform aside from a distribution of curved dark lines with diminished SHG intensity all across the image. These dark lines are the domain boundaries, where the SHG from neighboring domains causes destructive interference, as $\chi_{yyy}(T^{M+}) = -\chi_{yyy}(T^{M-})$. Therefore, the pattern in Fig. 4(a) corresponds to the distribution of the ferrotoroidic domain walls and, hence, of the domains in our NdB_4 sample.

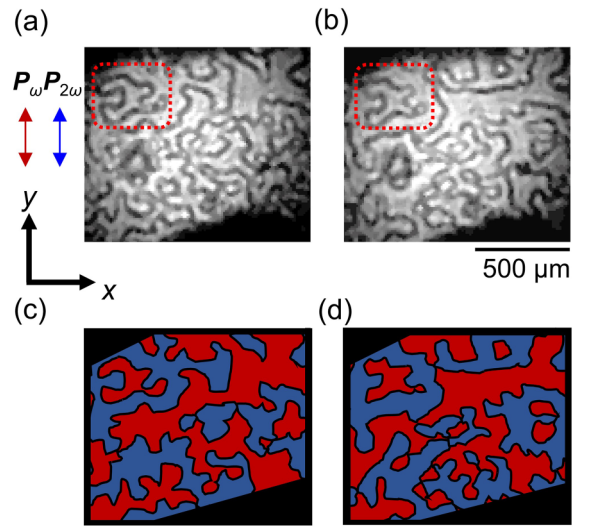


FIG. 4. SHG image obtained in the polarization setting of $\mathbf{P}_\omega \parallel \mathbf{P}_{2\omega} \parallel y$ at 10 K . The images of (a) and (b) are obtained after the first and second cooling run, respectively. The curved dark lines correspond to the ferrotoroidic domain boundaries. The domain surrounded by red dashed lines were memorized across the ordering temperature. Panels (c) and (d) show schematic illustrations of extracted domain structures from the domain-boundary maps shown in (a) and (b), respectively. The dark red and blue regions correspond to either T^{M+} or T^{M-} .

Figure 4(c) shows a sketch of the domain pattern extracted from the SHG map in Fig. 4(a). Note that although the domain pattern is clearly identified, the ferrotoroidic polarity of the respective domains cannot be uniquely associated by this SHG-map measurement. The domains are hundreds of micrometers in size, and everywhere they exhibit curved delimiters without directional preference. After obtaining the first image, the sample was heated up to 20 K ($> T_0$) and cooled down again to 10 K . Figures 4(b) and 4(d) show the resulting SHG map and the domain pattern, respectively, after this second cooling. Differences to Figs. 4(a) and 4(b) are observed in several areas, suggesting that the domains were reconstructed across the ordering temperature with only limited memory effects, visible, for example, in the top left part surrounded by red dashed lines in Figs. 4(a) and 4(b).

We argue that the SHG maps shown in Fig. 4 reflect ferrotoroidic domains as they were obtained in the setting $\mathbf{P}_\omega \parallel \mathbf{P}_{2\omega} \parallel y$, where only the toroidally arranged in-plane magnetic moments contribute to SHG. A SHG signal from χ_{yyy} is permitted by the ferrotoroidic order but does not exclude contributions from the out-of-plane magnetic moments. Therefore, we acquired a SHG image by rotating the polarization of the fundamental light and the SHG light simultaneously and performed a SHG polarization analysis. The measurements were done at 5 K . The intensity of all pixels within a single-domain area was averaged and plotted against the angle of the polarization of the fundamental light. Figures 5(a) and 5(b) show the SHG anisotropy data obtained on the two adjacent domains 1 and 2 [see the red and blue boxes in Fig. 5(e)] in the parallel-Nicols setting (the polarization of the fundamental light and the SHG light are

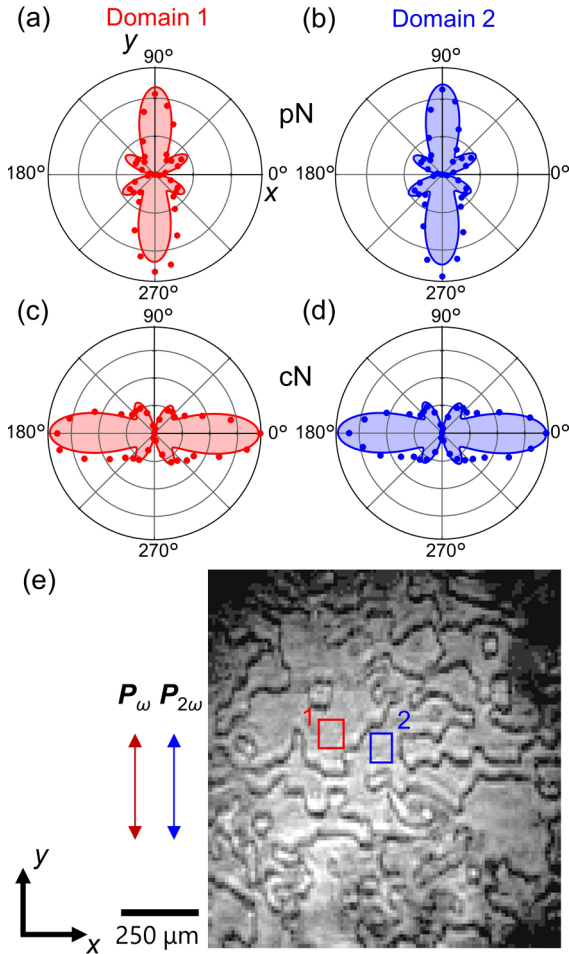


FIG. 5. SHG polarization analysis. (a)–(d) The intensity of SHG at 5 K in the two adjacent domains [areas in the red box (domain 1) and the blue box (domain 2) in panel (e)]. Panels (b) and (d) [(c) and (e)] show the SHG anisotropy obtained in parallel-Nicols (pN) setting and crossed-Nicols (cN) setting in domain 1 [domain 2], respectively. The data were obtained with rotating the polarization of the fundamental light and the SHG light simultaneously in either pN or cN setting. The red and blue curves show the results of the fitting. (e) SHG image obtained in the polarization setting of $\mathbf{P}_\omega \parallel \mathbf{P}_{2\omega} \parallel y$ at 5 K.

parallel, $\mathbf{P}_\omega \parallel \mathbf{P}_{2\omega}$), while Figs. 5(c) and 5(d) show those in the crossed-Nicols setting (the polarization of the fundamental light and the SHG light are orthogonal, $\mathbf{P}_\omega \perp \mathbf{P}_{2\omega}$). The obtained patterns do not exhibit a noticeable dependence on the choice of domain. They are fitted by assuming the tensor components derived from both the in-plane and out-of-plane magnetic moments, which yields normalized tensor components deriving from the in-plane magnetic moments as $\chi_{xxy} = 0.63 \pm 0.02$ (0.63 ± 0.02), $\chi_{yyy} = 0.83 \pm 0.02$ (0.84 ± 0.02), and $\chi_{yxx} = -0.90 \pm 0.01$ (-0.90 ± 0.01) for domain 1 (domain 2). Again, there is no significant difference between the tensor components of domain 1 and domain 2. On the other hand, the components deriving from the out-of-plane magnetic moments, χ_{xxx} , χ_{xyy} , and χ_{xyx} are zero within the

fitting errors and therefore at least ten times smaller than those from the in-plane magnetic moments. This is reasonable by considering that the tilting angle of magnetic moments at 5 K is about 8° [35] and the out-of-plane magnetic moments are 14% of the in-plane magnetic moments, leading to an approximately 50-fold difference in the SHG intensity between the in-plane and out-of-plane components ($0.14^2 \approx 0.02$). Thus, by considering that the SHG tensor components are well matched with those expected for the in-plane magnetic order, we conclude that the observed SHG signal constitutes a background-free representation of the ferrotoroidic domains in NdB_4 . SHG measurements in another setting sensitive to the out-of-plane components, such as using the *ab*-plane reflection, will be interesting future work for observations of magnetically induced ferroelastic and/or ferroaxial order and successive magnetic transitions at 7.0 and 4.8 K in NdB_4 .

Recently, antiferromagnetic domains in TbB_4 , a sister compound of NdB_4 , have been spatially visualized via nonreciprocal rotation of reflected light (NRR) [32]. NRR is allowed in systems with finite diagonal components of the linear ME tensor, such as TbB_4 (magnetic point group: $4/m'm'm'$) but not in systems free from such diagonal components, such as ferrotoroidic NdB_4 (magnetic point group: $2'/m$) [43–45]. Therefore, NRR cannot be applied to study ferrotoroidic order. On the other hand, the off-diagonal components of the ME tensor and the associated ferrotoroidic order and domains may be probed by nonreciprocal directional dichroism [14–17], which, however, is detected in transmission and thus not feasible in opaque metallic systems such as NdB_4 . Thus, SHG is the method of choice here because it is sensitive to ferrotoroidic order and domains in metallic systems.

In conclusion, we obtain images of the ferrotoroidic domain pattern of a metallic tetraboride, NdB_4 , by SHG. The domains were visualized via the observation of domain boundaries using the SHG interference between the domains with the opposite ferrotoroidic polarity. We note that the present study reveals the spontaneous formation of ferrotoroidic domains in a metallic material, whereas earlier studies on ferrotoroidic domains have been performed for insulating magnetoelectric materials. In these, the simultaneous application of electric and magnetic fields is required for domain switching [8, 16], whereas in metallic materials, it is predicted that domain switching is achieved by just applying electric current [20, 21]. Our findings hence constitute the preparation for such an experimental demonstration.

We thank J. Li, F. Wang, J. G. Horstmann, Y. Zemp, L. Forster, A. M. Müller, and T. Lottermoser for assistance with the experimental setup and fruitful discussions. The images of crystal structures were drawn using the software VESTA [46]. T.H. acknowledges support by JSPS KAKENHI Grant No. JP22J11247 and the “Young Researchers’ Exchange Programme between Japan and Switzerland 2022” under the “Bilateral Japanese-Swiss Science and Technology Programme.” T.K. acknowledges financial support by JSPS KAKENHI Grants No. JP19H05823 and No. JP21H04436. M.F. acknowledges financial support by the Swiss National Science Foundation under SNSF Project No. 200021_215423.

- [1] V. L. Ginzburg, A. A. Gorbatsevich, Y. V. Kopayev, and B. A. Volkov, *Solid State Commun.* **50**, 339 (1984).
- [2] V. M. Dubovik and V. V. Tugushev, *Phys. Rep.* **187**, 145 (1990).
- [3] A. A. Gorbatsevich and Y. V. Kopayev, *Ferroelectrics* **161**, 321 (1994).
- [4] H. Schmid, *Ferroelectrics* **252**, 41 (2001).
- [5] C. Ederer and N. A. Spaldin, *Phys. Rev. B* **76**, 214404 (2007).
- [6] N. A. Spaldin, M. Fiebig, and M. Mostovoy, *J. Phys.: Condens. Matter* **20**, 434203 (2008).
- [7] B. B. Van Aken, J. P. Rivera, H. Schmid, and M. Fiebig, *Nature (London)* **449**, 702 (2007).
- [8] A. S. Zimmermann, D. Meier, and M. Fiebig, *Nat. Commun.* **5**, 4796 (2014).
- [9] S. Gnewuch and E. E. Rodriguez, *J. Solid State Chem.* **271**, 175 (2019).
- [10] J.-P. Rivera, *Ferroelectrics* **161**, 147 (1994).
- [11] N. Mufti, G. R. Blake, M. Mostovoy, S. Riyadi, A. A. Nugroho, and T. T. M. Palstra, *Phys. Rev. B* **83**, 104416 (2011).
- [12] Y. Yamaguchi, T. Nakano, Y. Nozue, and T. Kimura, *Phys. Rev. Lett.* **108**, 057203 (2012).
- [13] J. Zhang, X. Wang, L. Zhou, G. Liu, D. T. Adroja, I. da Silva, F. Demmel, D. Khalyavin, J. Sannigrahi, H. S. Nair, L. Duan, J. Zhao, Z. Deng, R. Yu, X. Shen, R. Yu, H. Zhao, J. Zhao, Y. Long, Z. Hu *et al.*, *Adv. Mater.* **34**, e2106728 (2022).
- [14] V. Kocsis, K. Penc, T. Róhm, U. Nagel, J. Vít, J. Romhányi, Y. Tokunaga, Y. Taguchi, Y. Tokura, I. Kézsmárki, and S. Bordács, *Phys. Rev. Lett.* **121**, 057601 (2018).
- [15] T. Sato, N. Abe, S. Kimura, Y. Tokunaga, and T.-H. Arima, *Phys. Rev. Lett.* **124**, 217402 (2020).
- [16] K. Kimura, Y. Otake, and T. Kimura, *Nat. Commun.* **13**, 697 (2022).
- [17] Y. Sawada, S. Kimura, K. Watanabe, Y. Yamaguchi, T. Arima, and T. Kimura, *Phys. Rev. Lett.* **129**, 217201 (2022).
- [18] T. Jungwirth, X. Marti, P. Wadley, and J. Wunderlich, *Nat. Nanotechnol.* **11**, 231 (2016).
- [19] V. Baltz, A. Manchon, M. Tsoi, T. Moriyama, T. Ono, and Y. Tserkovnyak, *Rev. Mod. Phys.* **90**, 015005 (2018).
- [20] H. Watanabe and Y. Yanase, *Phys. Rev. B* **98**, 220412(R) (2018).
- [21] F. Thöle, A. Keliri, and N. A. Spaldin, *J. Appl. Phys.* **127**, 213905 (2020).
- [22] P. Wadley, B. Howells, J. Železný, C. Andrews, V. Hills, R. P. Campion, V. Novák, K. Olejník, F. Maccherozzi, S. S. Dhesi, S. Y. Martin, T. Wagner, J. Wunderlich, F. Freimuth, Y. Mokrousov, J. Kuneš, J. S. Chauhan, M. J. Grzybowski, A. W. Rushforth, K. W. Edmonds *et al.*, *Science* **351**, 587 (2016).
- [23] J. Godinho, H. Reichlová, D. Kriegner, V. Novák, K. Olejník, Z. Kašpar, Z. Šobáň, P. Wadley, R. P. Campion, R. M. Otxoa, P. E. Roy, J. Železný, T. Jungwirth, and J. Wunderlich, *Nat. Commun.* **9**, 4686 (2018).
- [24] S. Hayami, H. Kusunose, and Y. Motome, *Phys. Rev. B* **90**, 024432 (2014).
- [25] H. Saito, K. Uenishi, N. Miura, C. Tabata, H. Hidaka, T. Yanagisawa, and H. Amitsuka, *J. Phys. Soc. Jpn.* **87**, 033702 (2018).
- [26] A. Zalkin and D. H. Templeton, *Acta Crystallogr.* **6**, 269 (1953).
- [27] Z. Fisk, A. S. Cooper, P. H. Schmidt, and R. N. Castellano, *Mater. Res. Bull.* **7**, 285 (1972).
- [28] D. Brunt, G. Balakrishnan, D. A. Mayoh, M. R. Lees, D. Gorbunov, N. Qureshi, and O. A. Petrenko, *Sci. Rep.* **8**, 232 (2018).
- [29] S. W. Lovesey, J. Fernández Rodríguez, J. A. Blanco, and P. J. Brown, *Phys. Rev. B* **70**, 172414 (2004).
- [30] S. W. Lovesey, E. Balcar, K. S. Knight, and J. Fernández Rodríguez, *Phys. Rep.* **411**, 233 (2005).
- [31] H. Watanabe and Y. Yanase, *Phys. Rev. B* **98**, 245129 (2018).
- [32] K. Arakawa, T. Hayashida, K. Kimura, R. Misawa, T. Nagai, T. Miyamoto, H. Okamoto, F. Iga, and T. Kimura, *Phys. Rev. Lett.* **131**, 236702 (2023).
- [33] R. Watanuki, T. Kobayashi, R. Noguchi, and K. Suzuki, *J. Phys. Conf. Ser.* **150**, 042229 (2009).
- [34] H. Yamauchi, N. Metoki, R. Watanuki, K. Suzuki, H. Fukazawa, S. Chi, and J. A. Fernandez-Baca, *J. Phys. Soc. Jpn.* **86**, 044705 (2017).
- [35] N. Metoki, H. Yamauchi, M. Matsuda, J. A. Fernandez-Baca, R. Watanuki, and M. Hagihala, *Phys. Rev. B* **97**, 174416 (2018).
- [36] K. Aizu, *J. Phys. Soc. Jpn.* **27**, 387 (1969).
- [37] H. Schmid, *J. Phys.: Condens. Matter* **20**, 434201 (2008).
- [38] M. Yatsushiro, H. Kusunose, and S. Hayami, *Phys. Rev. B* **104**, 054412 (2021).
- [39] M. Fiebig, V. V. Pavlov, and R. V. Pisarev, *J. Opt. Soc. Am. B* **22**, 96 (2005).
- [40] R. R. Birss, *Symmetry & Magnetism* (North-Holland, Amsterdam, 1966).
- [41] M. Fiebig, T. Lottermoser, D. Fröhlich, and S. Kallenbach, *Opt. Lett.* **29**, 41 (2004).
- [42] Y. Kaneko and Y. Tokura, *J. Cryst. Growth* **533**, 125435 (2020).
- [43] R. M. Hornreich and S. Shtrikman, *Phys. Rev.* **171**, 1065 (1968).
- [44] B. B. Krichevstov, V. V. Pavlov, R. V. Pisarev, and V. N. Gridnev, *J. Phys.: Condens. Matter* **5**, 8233 (1993).
- [45] B. B. Krichevstov, V. V. Pavlov, R. V. Pisarev, and V. N. Gridnev, *Phys. Rev. Lett.* **76**, 4628 (1996).
- [46] K. Momma and F. Izumi, *J. Appl. Crystallogr.* **44**, 1272 (2011).